PS/LPI/Note/85-10
13.6.1985

# RF MEASUREMENTS ON THE LIL-V BUNCHER AT CERN

A. Bellanger, M. Croizat, S. Kulinski, D. Warner

## 1. Introduction

The installation of the 30 MeV buncher V at CERN created a good opportunity to make the RF measurements of its accelerating structure. They were thought to be complementary to those made by LAL [2, 3]. The following measurements were proposed:

1. Measurement of cavity input impedance together with cavity matching to the wave guide.

2. Mode spectrum measurements - to obtain a dispersion curve with possible stop-bands.

3. Axial distribution of amplitude $E_z$ of electric field by perturbation method.

4. Perturbation measurements of axial field distribution on adjacent modes.

## 2. Measurements

### 2.1 Input impedance and coupling

The measurements were made by reflection using a 8410B network analyser. The schematic diagram for these measurements is given in Figure 1. The conditions of measurements were :

- atmospheric pressure $P_a$ = 1043 mb
- temperature $t$ = 14°C
- relative humidity $H$ = 73%

The measured resonance frequency was $f_o$ = 2998.530 MHz. It happened, by chance, that it was almost precisely equal to the nominal working frequency fr = 2998.5 MHz. This frequency should be obtained under vacuum and at the temperature 31.3°C. It is known [3] that passing from vacuum to atmospheric pressure decreases the resonant frequency by about 950 kHz, and decreasing of temperature by 1°C increases the frequency by about 50 kHz. As a result we obtained that changes of pressure and temperature almost compensated each other.

The results of measurements were displayed on the Smith Chart. The typical changes of input impedance as a function of frequency sweep are presented on Fig. 2. It can be seen from this figure that coupling coefficient $\beta$ is practically equal to 1. More precise measurements with 20 dB expanded scale gave for coefficient of reflection ($\Gamma$) $\approx$ 0.016 and for coupling $\beta \approx 1.031$. It means that the accelerating structure is critically coupled.

This value of $\beta$ disagrees with the results of coupling measurements made by LAL in 1980 at CGR-MeV, when $\beta$ was found to be equal to 1.4. However, according to LAL (J.C. Bourdon, private communication) since then the coupling was changed by CGR-MeV and was made closer to 1 by corrections in the power input coupler. We will return to this point below when discussing the results of perturbation measurements.

A few step by step measurements giving changes of input impedance Z as a function of frequency were made and are given in Table I and are also presented at Fig. 3.

Table I shows also the values of Q-factor calculated with the use of known formula :

$$Q = \frac{f_0 . tg\ \phi}{2.\Delta f}$$

where : $f_0$ = resonant frequency
$\phi$ = phase angle of impedance corresponding to the frequency change $\Delta f = (f - f_0)$.

As it is seen from this table the value of Q decreases with increasing $\phi$ (or $\Delta f$), from 13.052 for $\phi \approx 26^o$ ($\Delta f \approx 56$ kHz) to 10.164 for $\phi \approx 43.0$ corresponding practically to half power points. According to Fig. 2, these changes are due to the influence of neighbouring resonances which are relatively close to $f_0$. Since this influence is greater for larger $\Delta f$ ($\approx \phi$) it seems reasonable to take for Q the value obtained for small $\Delta f$. In our case Q will then be equal to 13000 which agrees with LAL measurements giving Q values within limits (11250 : 15000).

## 2.2 Modes measurements

The aim of these measurements was to find the large number of resonant frequencies corresponding to the modes excited in the accelerating structure, and to draw afterwards the dispersion curve. The total number of modes is equal to the number of cells from which the structure is composed. In our case this number is equal to 69 ( 2 cells $\pi/2$ at both ends of the structure, 2 times 22 accelerating cavities of the type 2/3 $\pi$ and 23 coupling cavities).

The measurements were made in the transmission mode. The structure was excited by synthesized signals generator HP 8672A through the power input and the signal was received by one of two loops. A schematic diagram for these measurements is given on Fig. 4.

Conditions during the measurements :

- pressure (atmospheric) $P_a$ = 1043 mb
- temperature $t^a$ = 14°C
- resonant humidity H = 54%
- resonant frequency of the mode 2/3 $\pi$ $f_0 = f_{2/3\pi}$ = 2998.526 MHz

It should be stressed that although the temperature of the structure was not stabilized by the water circuit, the temperature in the tunel was rather stable. The changes of the temperature during the day never exceeded

1°C giving (together with pressure and humidity variations) the changes in resonant frequency of the order of 10-15 kHz.

Since the amplitudes of neighbour resonances were sometimes different by (40-50) dB, special care was taken to detect also very weak resonances. It appeared very helpful for this purpose to display the cavity responses simultaneously on the Smith Chart HP 8414A and on the phase-magnitude display HP 8412A.

The results of these measurements are given in Table II. As it is seen from this table, 49 resonances out of 69 were found. In fact with the arrangement given on Fig. 4 the number of modes which could be detected is smaller and is equal to a number of cells included between the power input which is placed in volume 62-63 (accelerating cavity 43) and the loop 2 placed in volume 6-7 (accelerating cavity 6). As a result there are 8 cavities missed at the beginning (5 accel., 3 coupling) and 5 cavities missed at the end (3 accel., 2 coupling) so that total number of modes which could be detected is 56, and only 7 modes were not found. As it will be seen later all the 23 resonances between modes 1/3 $\pi$ and 2/3 $\pi$ were found. This was very important since it helped us in a proper assignment of the frequencies to the phase shifts of the modes.

In the case of a triperiodic structure, like that of the buncher V, there are generally three pass-bands separated by two stop bands at 1/3 $\pi$ and 2/3 $\pi$ modes [1]. The stop band at 2/3 $\pi$ mode is more dangerous since it is the working mode of our structure. The existence of the stop bands can be easily seen from the dispersion curve. To draw this curve it is necessary to know the values of resonant frequencies for the 69 values of phase shifts given by

$$\phi_n = \frac{n\pi}{68} \qquad n = 0, 1, \ldots\ldots 68$$

Since in our case we did not find the frequencies of all modes a care must be taken to a proper assignment of the frequencies to the phase shift $\phi_n$. Happily enough we knew all the modes in the pass-band between 1/3 $\pi$ and 2/3 $\pi$ and this enabled us the construction of the dispersion curve shown on Fig. 5. According to this curve there is no stop band for the resonant mode 2/3 $\pi$, but there exists a stop band of the order of 10 MHz for the mode 1/3 $\pi$. Note that only a small number of modes (9 out of 23) were found below the mode $\pi/3$.

Fig. 6. presents the modes measured in LAL at Orsay in March 1985. The agreement is good.

Fig. 7. gives the dispersion curve for the prototype of our structure [1]. Again a good agreement is to be noted between two curves with similar stop band for 1/3 $\pi$ mode, and similar limits between mode 0 and $\pi$.

### 2.3 Perturbation measurements

We intended to make two kinds of perturbation measurements :

a) Measurements in auto-oscillating circuit, where the cavity is the frequency determining element in auto-oscillating circuit formed, together with an amplifier and adjustable phase-shift, into closed loop.

b) Indirect measurements of change in cavity resonant frequency by measuring the phase shift (near the resonance) between the input wave and r.f. field in the cavity.

The measuring set-up for the auto-oscillation is given on Fig. 8. We did not succeed to make the measurements. The most probable reason for this was the lack of sufficiently powerful amplifier. We had only 30 dB gain amplifier with power output of 1 Watt and it was not sufficient to excite the auto-oscillations in the circuit which contained also a loop with coupling of the order of -50 dB.

A schematic diagram for perturbation measurements with the aid of phase shift is shown in Fig. 9. The principles of these measurements are based on the "Slater Perturbation Theorem [4, 5, 7], which can be written in the form :

$$\frac{\delta f}{f_0} = \frac{k \int (\mu H^2 - \varepsilon E^2)\, d\tau}{4U}$$

where

$\delta f = f - f_0$ - is the frequency change caused by perturbing element

$E$, $H$ - electric and magnetic field intensities in cavity

$\varepsilon$, $\mu$ - dielectric constant and magnetic permeability of the medium in the cavity

$U = \int (\mu H^2 + \varepsilon E^2)\, dv$ - average stored energy of cavity

$k$ - constant depending upon the shape of perturbing object

The integral is taken over the perturbed volume. In our case we wish to measure the axial electric field distribution. In the vicinity of axis we have : $H \approx 0$, $E \approx E_z$ and for the case of metallic sphere (bead) of radius a the perturbation of frequency is given by [5] :

$$\frac{\delta f}{f_0} = -3 \cdot \frac{4}{3} \pi a^3 \frac{E_z^2}{4U} = -\pi a^3 \frac{E_z^2}{U}$$

As a result we obtained that the square of axial electric field amplitude $E_z^2$ is proportional to the frequency perturbation $\delta f$.

On the other hand in the vicinity of resonance there is the following relation :

$$\operatorname{tg} \delta\gamma = \frac{2 Q_L \delta f}{f_0}$$

between the phase shift $\delta\gamma$ of the r.f. field in the cavity and the frequency shift $\delta f = (f - f_0)$. Were $Q_L$ is the loaded Q of the cavity, and $f_0$-resonant frequency. For small $(\delta\gamma) \ll 1$ we have $\operatorname{tg} \delta\gamma \approx \delta\gamma$ so that there exists a linear

relation between change in $\delta\gamma$ and $\delta f$. Usually then, for convenience of calibration, one prefers to stay within the limits of small $\delta\gamma$ and correspondingly small $\delta f$. E.g. for change of $\delta\gamma$ in the range $\pm 10^{\circ}$ the change in phase is linear in frequency to about 1%. Assuming for our buncher $Q_L = Q_0/(1+\beta) \approx 7.500$, we obtain variations of frequency $(\delta f) \approx 35$ kHz for change $\delta f \approx \pm 10^{\circ}$. We shall see below that during the measurements we had $(\delta f) \approx 20$ kHz so that we stayed in the linear region of phase changes with frequency.

Conditions during measurements :

- pressure (atmospheric) $P_a$ = 1045 mb
- temperature $t$ = 14°C
- relative humidity = 65%
- resonant frequency :
  without the nylon string = $f_0$ = 2998.535 MHz
  with the nylon string = $f$ = 2998.521 MHz
  metallic perturbing bead $\Phi$ = 2.5 mm
  nylon string $\Phi$ = 0.1 mm

Remark :

As it was already mentioned there are two measuring loops installed in the buncher : the first (referred to as loop 1) is placed at the exit end in the accelerating cavity 45 and has the coupling -57 dB, the second (loop 2) installed at the beginning in the accelerating cell 6 has the coupling about -50 dB (see Fig. 10a).

It was noticed at the beginning of the measurements that the results depend strongly on the loop used as reveiver. Loop 2 gave always the resonant frequency lower by about 100 kHz and more distorted field distribution.

The possible explanation of this experimental fact will be given below, but knowing it we decided to make practically all measurements with the aid of loop 1.

Following measurements were made :

1) Perturbation on the working frequency $f_0 = f_{(2/3)\pi}$ to obtain axial field distribution. The results of these measurements (made with the aid of the loop 1) are shown on Fig. 10 where the variations of $\Delta f \approx E_z^2$ along the axis of the structure are presented. Note that the peaks correspond to the field in the accelerating cells. The field in the coupling cells is small, theoretically zero. Table III (constructed on the basis of Fig. 10) gives some details concerning the distribution of axial electric field $E_z$ in accelerating cavities. Both Fig. 10 and Table III show rather large variations of the axial field distribution especially at the ends of the structure. For instance at the exit end of the beam (near the power input) variations in $E_z$ amplitude exceed 20%. In the central part they are smaller than 10%. The values obtained by LAL [2] are about ± 5% at the beginning and in the middle and ± 15% at the exit (see Fig.11). These values should be compared with those given by Bensussan et al. [1] for the prototype structure. According to them the field level at the ends was about 10% below the average value and the field flatness was better than ± 2% elsewhere. This field distribution is just opposite to ours and LAL results since we have higher field level at the ends and lower in the middle.

Another striking feature of our field distribution is that as a rule every second accelerating cell has smaller field amplitude. As we shall see this feature is characteristic for all measurements. The possible explanation of this will be given below.

Fig. 12 shows the results of perturbation measurements obtained with the aid of loop 2. The axial field distribution is now completely different in comparison with the case of loop 1. E.g. instead of a large maximum of the field level at the exit end of the structure a minimum is now produced. Also a very large difference in excitation of every second accelerating cell is now visible. In most cases changes in $\delta f \approx E_z^2$ in these cells are about 50% smaller.

2) Stability of electric field distribution in the structure against frequency perturbations at the ends.

The perturbation was made by inserting a small piece of metal into the first or last cell correspondingly. Four measurements were made : shift of the resonant frequency of the whole structure by $\Delta f$ = -63 kHz, -130 kHz and -251 kHz by perturbation at the beginning and shift $\Delta f$ = -40 kHz by perturbation at the end of the structure.

n the structure was much more sensitive to a perturbation at the exit end It was noted that the field distribution ithan to a perturbation at the beginning of the structure. The possible explanation of this is that both power input and loop 1 are in the vicinity of this end.

Fig. 13 and 14 present the results obtained for the cases of $\Delta f$ = -63 kHz and $\Delta f$ = -130 kHz frequency perturbations at the beginning and Fig. 15 the case of $\Delta f$ = -40 kHz at the end. It is interesting to notice that again every second an accelerating cell is more influenced by these perturbations.

Before further information we should say a few words on the periodicity of a triperiodic structure. Per period we have two groups of accelerating cells which can be numbered e.g. 3n-2, 3n-1, and one coupling cell 3n. Another simple way to discern these two groups is by consecutive numbering the accelerating cells. Then the odd cells form one group and the even cells the other (see Fig. 10a).

Analysis of Figs. 13, 14 and 15 show that if the source of frequency perturbation is in one group of cells, it is the other type group of cells that exhibits the largest amplitude variations. Similar results were found by S.O. Schriber [6].

From Figs. 13 and 14 it is evident that the difference in the $E_z^2$ amplitudes between the two groups of accelerating cells is proportional to the disturbance $\Delta f$. It was even more clear for the case of $\Delta f$ = -251 kHz (not shown on the picture) where one group of cells was almost not excited.

A very interesting case is presented on Fig. 15. Although the perturbation of the exit $\pi/2$ cell changed the frequency of the structure only by $\Delta f$ = -40 kH, the axial field distribution is completely changed. The main differences in comparison with unperturbed cases are :

1) Except for 3 last cells the field amplitudes distribution became more uniform and the field level variations do not exceed 10%.

2) Since it was the even numbered (46) cell perturbed, all odd-numbered cells are more infuenced by this perturbation.

3) 40 kHz frequency shift was enough to overcome other possible perturbations which distorted "unperturbed" field distribution.

The discussion of the results presented on Figs. 13, 14 and 15 shows then that the structure is rather sensitive to frequency perturbations, and that this is the exit end which is more vulnerable for these perturbations.

Knowing the influence of frequency disturbance on the axial field distribution we can try to explain the curves shown on Figs. 10 and 12. We start with Fig. 12 which is easier to interpret. Since the difference in curves presented on Fig. 10 and 12 is caused by use of loop 2 instead of loop 1 it seems reasonable to look for the reason in this difference in loop 2. We know that the loop 2 has stronger coupling, to the structure than loop 1 and that it is placed in an even cavity (6) then it should influence mostly the odd cavities. Fig. 12 verifies this assumption.

The case presented on Fig. 10 is a little more complicated. An inspection of the distribution curve shows that there exist now two different parts in field distribution. From the beginning up to about 25 accelerating cell, the odd cells are more distorted. From the cell 26 up to the end the even cells are more influenced. This last part of the curve can be explained quite easily by perturbations caused by loop 1 at cell 45 and r.f. power input at cell number 43 which produce larger effect in even cells.

Then another part of that curve can be explained by assumption that there exist also other perturbation e.g. at the beginning of the structure which perturbs the frequency of the even cells so that the field amplitudes of odd cells are more influenced. Again it can be the frequency shift caused by loop 2 in cavity 6 that is responsable for this. In the middle both effects add to each other and the field amplitudes of both groups of cells are approximately equal, but somewhat smaller than at the ends.

3. Perturbation at the adjacent modes

The $E_z^2$ field amplitude distributions were also found for the 3 closest adjacent modes of 2/3 $\pi$ mode. Results of the measurements are shown in Figs. 16, 17 and 18.

It is seen from Figs. 16 and 17 that the field distribution for the two closest frequencies resembles the $TM_{01n}$ mode, one passing through zero of electric field $E_z$ along the z-axis. Assuming that we have (to the first approximation) cyclindrical cavities excited in the mode $TM_{01n}$, we obtain for the frequency $f_{01n}$ the expression:

$$f_{01n} = f_0 \sqrt{1 + \left(\frac{n\pi a}{2.405\, L}\right)^2}$$

where $f_0$ is the frequency of the mode 2/3 $\pi$ and is equal to 2998.5 MHz.

Inserting L = 2.244 m, a ≈ 4.12 cm for our buncher we obtain :

$$f_{011} = 2999.361 \text{ MHz}$$

whereas the measured value of the first higher frequency was 2999.29, which agrees rather well.

Perturbation on the second lower frequency shows two minima in $E_z$ field distribution along the z-axis (Fig. 18).

Discussion and conclusions

1) The structure is critically coupled to the power supply circuit.

2) Dispersion curve shows that there is no stop-band at the resonant 2/3 π mode. On the contrary, there is a stop-band of the order of 10 MHz at 1/3 π mode.

3) Rather large variations in the $E_z$ field distribution along the structure exist. They are of the order of ± 10% at the beginning and in the middle and exceed 20% at the end of the structure.

4) The structure is sensitive to the frequency perturbations. The perturbations at one end of the structure causing the frequency change of the order of (40-60) kHz change substantially the electric field distribution along the axis. For comparison: the metallic bead with the diameter Φ = 2.5 mm used for perturbation measurements caused a frequency change of about 20 kHz.

5) According to Figs. 10 and 11, both CERN and LAL measurements show the largest variations in field distributions at the end of the structure. A possible reason for this is break of symmetry in the end cells in comparison with other cells. The end cells have only cells on one side with which they can couple, this requires a very careful tuning of end cells.

   The additional perturbations exist at the exit end caused by power input coupling slot in accelerating cell 43 and loop 1 placed in accelerating cell 45, making the tuning even more difficult especially for triperiodic structure. According to Bensussan [1] and Schriber [6] the fault in coupling constant, even if it is localized in one place, can be reflected throughout the full length of the coupled system in the triperiodic structure. E.g. Bensussan wrote: "The presence of coupler disturbs noticeably the field distribution along the structure. The coupling cell to the r.f. source must be separately tuned to maintain good field flatness everywhere. Its frequency depends on the coupling aperture".

   The coupling iris in the coupling cell was changed between the LAL (Fig. 11) and the CERN (Fig. 10) measurements in order to decrease coupling coefficient β from 1.4 to 1.0. Given the sensitivity of the field distribution to perturbations and especially to the r.f. power coupler, this can explain the differences in results on field distribution obtained at LAL and at CERN.

Acknowledgements

The authors would like to express their gratitude to LAL-Orsay for help in preparation of the measurements.

The discussions with R. Belbéoch, J.C. Bourdon and C. Chaput of LAL as well as those with K. Hübner of CERN, who helped also in the organization of the experiment, are gratefully acknowledged.

## REFERENCES


1. A. Benussan et al., "High Power Standing Wave Triperiodic Structure for Positron Acceleration NIM 118 (1974), 349-355.

2. J.C. Bourdon, J. Rodier, "Compte-Rendu des Mesures HF sur le Groupeur de la Station d'Essais LAL/PI/80-87.

3. J.C. Bourdon, J. Rodier, "Groupeur-V, Mesures des Modes", Orsay le 14. 03 1985.

4. E.L. Ginzton, "Microwave Measurements", Mc. Graw Hill Book Company 1957.

5. L.C. Maier Jr., J.C. Slater, "Field Measurements in Resonant Cavities", J. Applied Physics 23, 1, pp. 68-77, 1952.

6. S.O. Schriber, "Comparison of Standing Wave Accelerators Operating in the $2/3\pi$ and $\pi/2$ modes", IEEE Tran. on Nucl Sci, Vol. NS-22, No 3, June 1975.

7. D. Warner, "Cavity Field Measurements by Perturbation: Some Requirements for a Computerised System", PS/LIN Note 76-2.

TABLE I

Accelerating Structure Input Impedance

in the Vicinity of the Resonant Frequency $f_0$ = 2998.53 MHz

| f(MHz) | $\frac{z}{z_o} = R + jx$ | $z = \lvert z \rvert e^{j\phi}$ | $Q = f_o \cdot tg\left(\frac{\phi_+ + 1\phi_- - 1}{2}\right)/(f_+ - f_-)$ |
|---|---|---|---|
| 2998.667 | 0.4 - j 0.35 | $0.5315\ e^{-j\ 41.19}$ | |
| 2998.617 | 0.6 - j 0.4 | $0.72\ e^{-j\ 33.69}$ | |
| 2998.554 | 0.8 - j 0.039 | $0.89\ e^{-j\ 25.983}$ | Q = 13 052 |
| 2998.530 | 1.03 | $1.03\ c^{jo}$ | Q = 12 054 |
| 2998.472 | 0.8 + j 0.39 | $0.89\ e^{j\ 25.983}$ | Q = 10 614 |
| 2998.441 | 0.6 + j 0.45 | $0.75\ e^{j\ 36.87}$ | |
| 2998.391 | 0.4 + j 0.4 | $0.565\ e^{j\ 45}$ | |

TABLE II

Resonant Frequencies of Modes

| Frequency MHz | | Frequency MHz | | Frequency MHz | |
|---|---|---|---|---|---|
| 1 | $f_{\frac{2}{3}\pi}$ = 2998.526 | | $f_{\frac{2}{3}\pi}$ = 2998.52 | 1 = | $f_{\frac{2}{3}\pi}$ = 2971.560 |
| 2 | 2997.663 | 1 | 2999.290 | 2 | 2970.660 |
| 3 | 2996.795 | 2 | 3000.096 | 3 | 2969.690 |
| 4 | 2997.937 | 3 | 3000.882 | 4 | 2968.910 |
| 5 | 2995.039 | 4 | 3001.382 | 5 | 2967.920 |
| 6 | 2994.035 | 5 | 3002.099 | 6 | 2967.00 |
| 7 | 2993.117 | 6 | 3002.740 | 7 | 2966.230 |
| 8 | 2992.222 | 7 | 3003.342 | 8 | 2965.600 |
| 9 | 2991.186 | 8 | 3003.967 | 9 | 2965.00 |
| 10 | 2990.248 | 9 | 3004.608 | | - - - - |
| 11 | 2989.643 | 10 | 3005.151 | | 2949.00? |
| 12 | 2988.659 | 11 | 3005.661 | | |
| 13 | 2987.860 | 12 | 3006.179 | | |
| 14 | 2986.921 | 13 | 3006.610 | | |
| 15 | 2986.011 | 14 | 3007.368 | | |
| 16 | 2985.108 | 15 | 3008.060 | | |
| 17 | 2984.157 | 16 | 3009.000 | | |
| 18 | 2983.349 | 17 | 3010.875 | | |
| 19 | 2982.638 | | | | |
| 20 | 2982.043 | | | | |
| 21 | 2981.553 | | | | |
| 22 | 2981.253 | | | | |
| 23 | 2981.013 | | | | |

## TABLE III

PERTURBATION MEASUREMENT OF AXIAL FIELD DISTRIBUTION

| Accel Cell No | $\Delta f \sim E_z^2$ | $\frac{E_z}{E_{z\,av}} = \sqrt{\frac{\Delta f}{\Delta f_{av}}}$ | $\frac{E_z}{E_{z\,av}} \cdot E_{zt}$ | Accel Cell No | $\Delta f \sim E_z^2$ | $\frac{E_z}{E_{z\,av}} = \sqrt{\frac{\Delta f}{\Delta f\ av}}$ | $\frac{E_z}{E_{z\,av}} \cdot E_{z\,th}$ |
|---|---|---|---|---|---|---|---|
| 1 | 7.0 | 1.0034 | 25.086 | 25 | 62.5 | 0.948155 | 23.704 |
| 2 | 76.5 | 1.0490 | 26.225 | 26 | 67.0 | 0.981696 | 24.542 |
| 3 | 64.5 | 0.96321 | 24.080 | 27 | 66. | 0.9743425 | 24.359 |
| 4 | 78.5 | 1.06261 | 26.565 | 28 | 64.5 | 0.963206 | 24.080 |
| 5 | 68.5 | 0.992624 | 24.816 | 29 | 66.0 | 0.974342 | 24.359 |
| 6 | 78.0 | 1.059222 | 26.481 | 30 | 66.0 | 0.9743425 | 24.359 |
| 7 | 64.5 | 0.963207 | 24.080 | 31 | 69. | 0.9962405 | 24.9060 |
| 8 | 74.5 | 1.035846 | 25.880 | 32 | 65. | 0.9669329 | 24.173 |
| 9 | 58.0 | 0.9133845 | 22.835 | 33 | 74. | 1.031705 | 25.793 |
| 10 | 70.5 | 1.007011 | 25.175 | 34 | 63. | 0.951940 | 23.799 |
| 11 | 58.5 | 0.917313 | 22.933 | 35 | 76. | 1.045554 | 26.139 |
| 12 | 7.1 | 1.015757 | 25.264 | 36 | 61. | 0.9367088 | 23.418 |
| 13 | 61.5 | 0.94054 | 23.513 | 37 | 75.5 | 1.042109 | 26.053 |
| 14 | 70 | 1.00343 | 25.086 | 38 | 60. | 0.928999 | 23.225 |
| 15 | 62 | 0.9443555 | 23.609 | 39 | 80. | 1.072715 | 26.818 |
| 16 | 68.5 | 0.9926244 | 24.816 | 40 | 61.5 | 0.940539 | 23.513 |
| 17 | 59 | 0.9212249 | 23.031 | 41 | 83 | 1.092644 | 27.316 |
| 18 | 63 | 0.9519408 | 23.779 | 42 | 64.5 | 0.9632068 | 24.080 |
| 19 | 59 | 0.92122 | 23.031 | 43 | 94.0 | 1.162796 | 29.070 |
| 20 | 63.5 | 0.9557109 | 23.893 | 44 | 98.5 | 1.1903037 | 29.758 |
| 21 | 60.5 | 0.9328619 | 23.322 | 45 | 103.0 | 1.217189 | 30.430 |
| 22 | 64.5 | 0.9632068 | 24.080 | 46 | 86. | 1.112215 | 27.805 |
| 23 | 63.0 | 0.95194 | 23.799 | | | | |
| 24 | 64.5 | 0.9632068 | 24.080 | | | | |

$\sum \Delta f = 3198$

$\Delta f_{av} = \frac{\sum \Delta f}{N} = 69.521739$

$E_z$ theoretical = 25 MV/m = $E_{zt}$

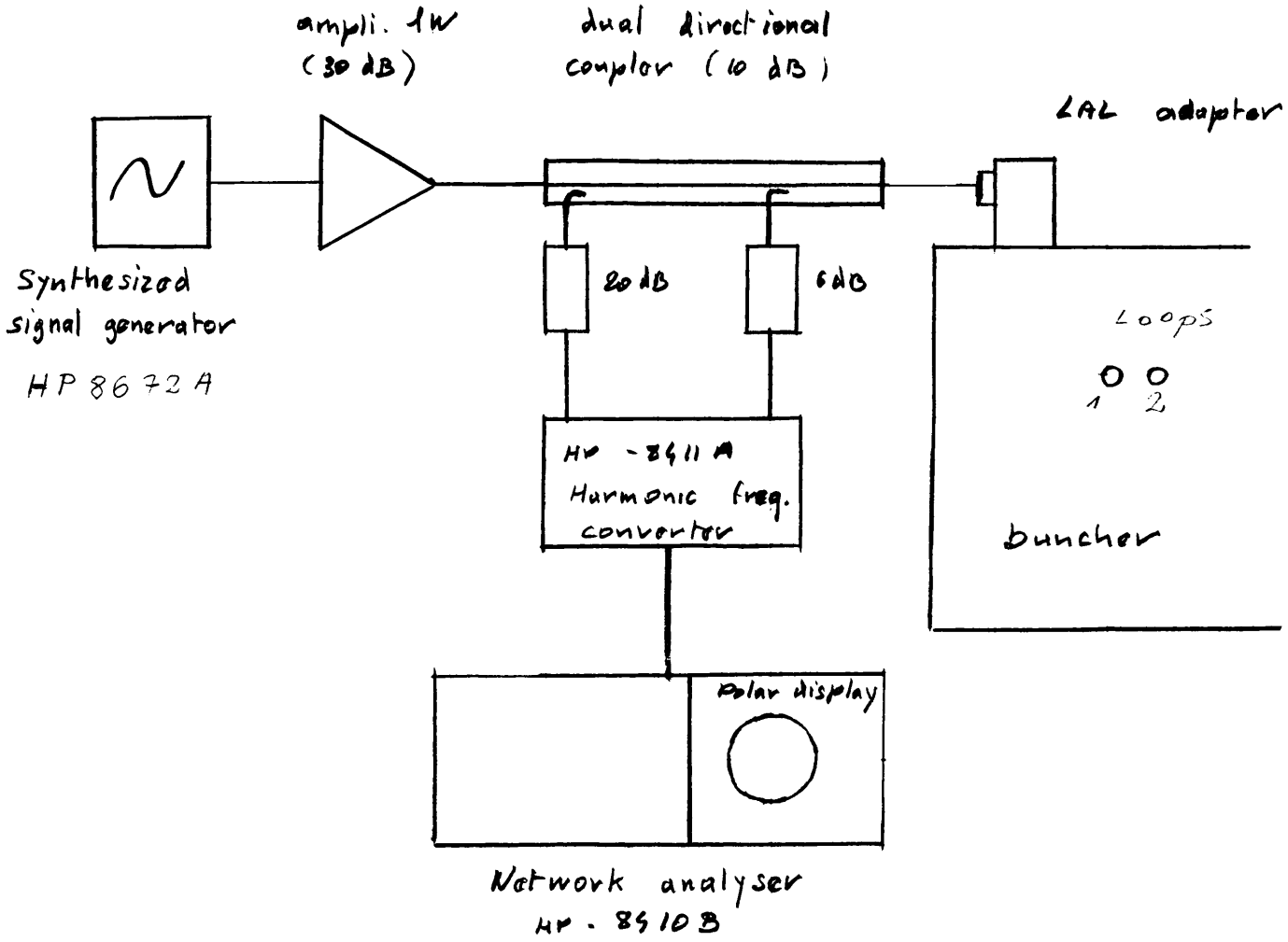


FIG.I. SCHEMATIC DIAGRAM FOR INPUT IMPEDANCE AND COUPLING MEASUREMENTS.

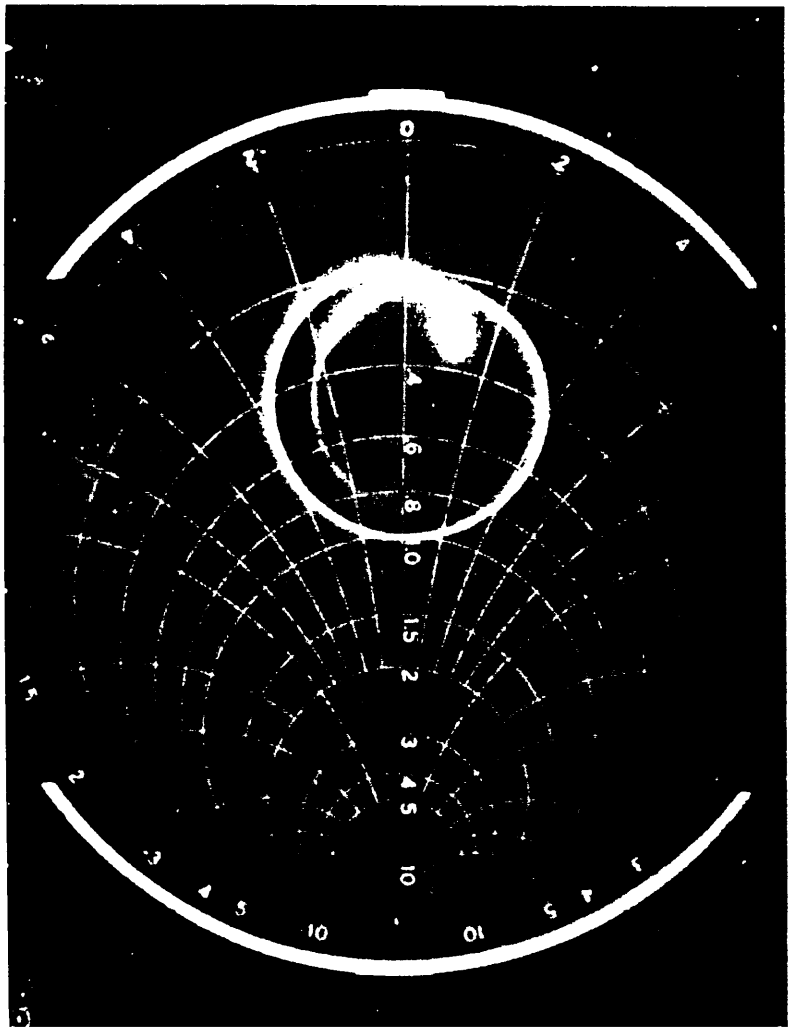

FIG . 2 INPUT IMPEDANCE FOR THE BUNCHER ACCELERATING STRUCTURE

| NAME | TITLE | DWG. NO. |
|---|---|---|
| SMITH CHART FORM 5301-7560-N | GENERAL RADIO COMPANY, WEST CONCORD, MASSACHUSETTS | DATE |

## IMPEDANCE OR ADMITTANCE COORDINATES

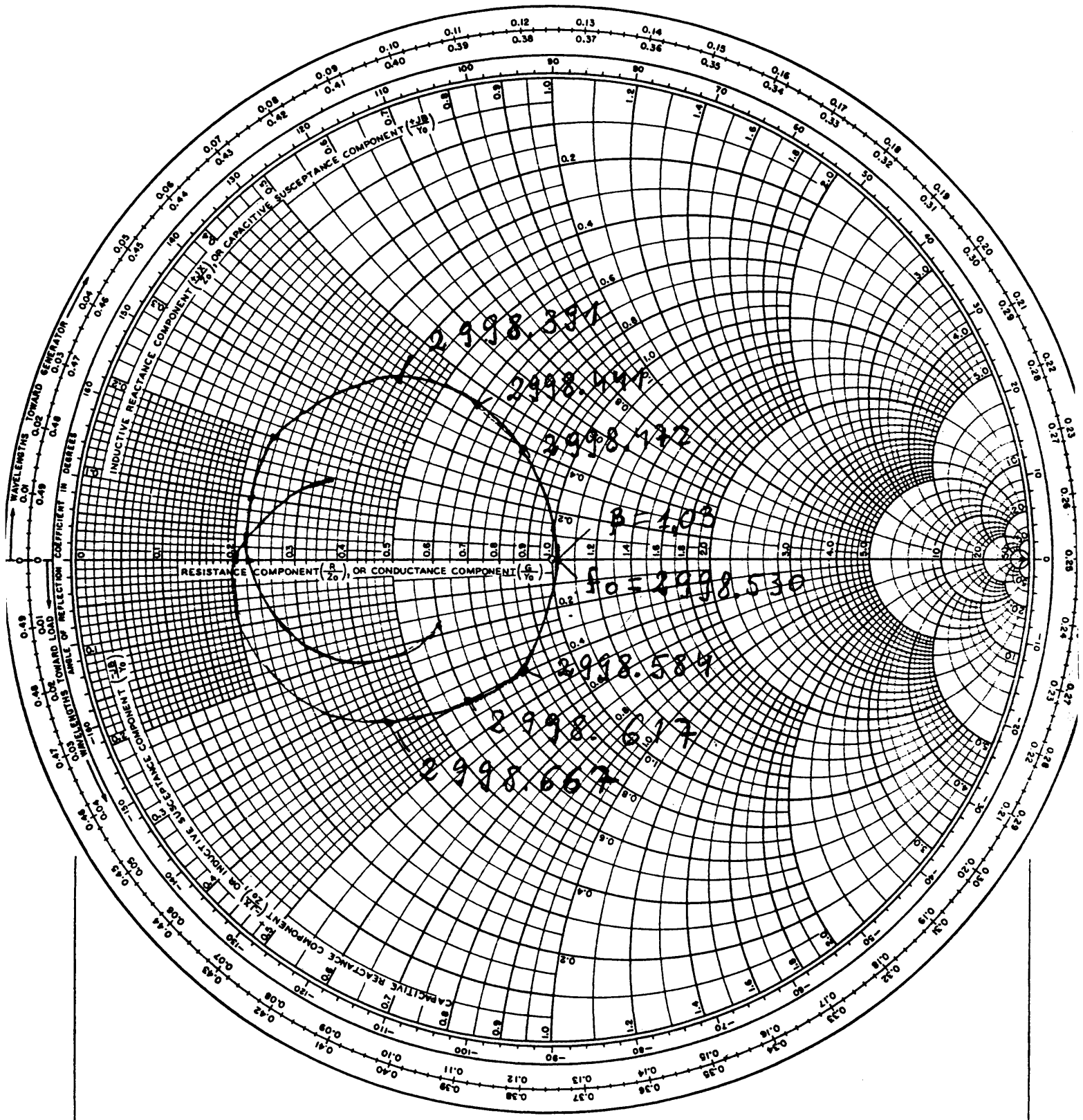


FIG. 3 CAVITY INPUT IMPEDANCE IN THE VICINITY OF RESONANT FREQUENCY $F_0$ = 2998.53 MHz

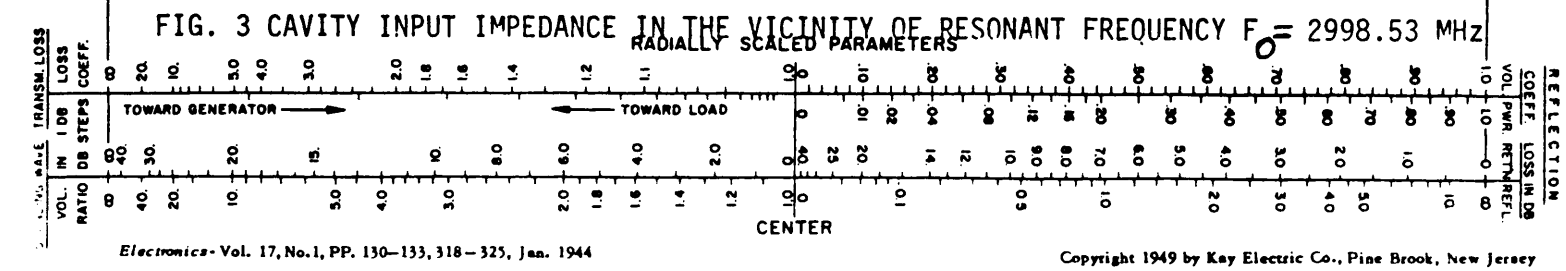


*Electronics*- Vol. 17, No. 1, PP. 130–133, 318–325, Jan. 1944

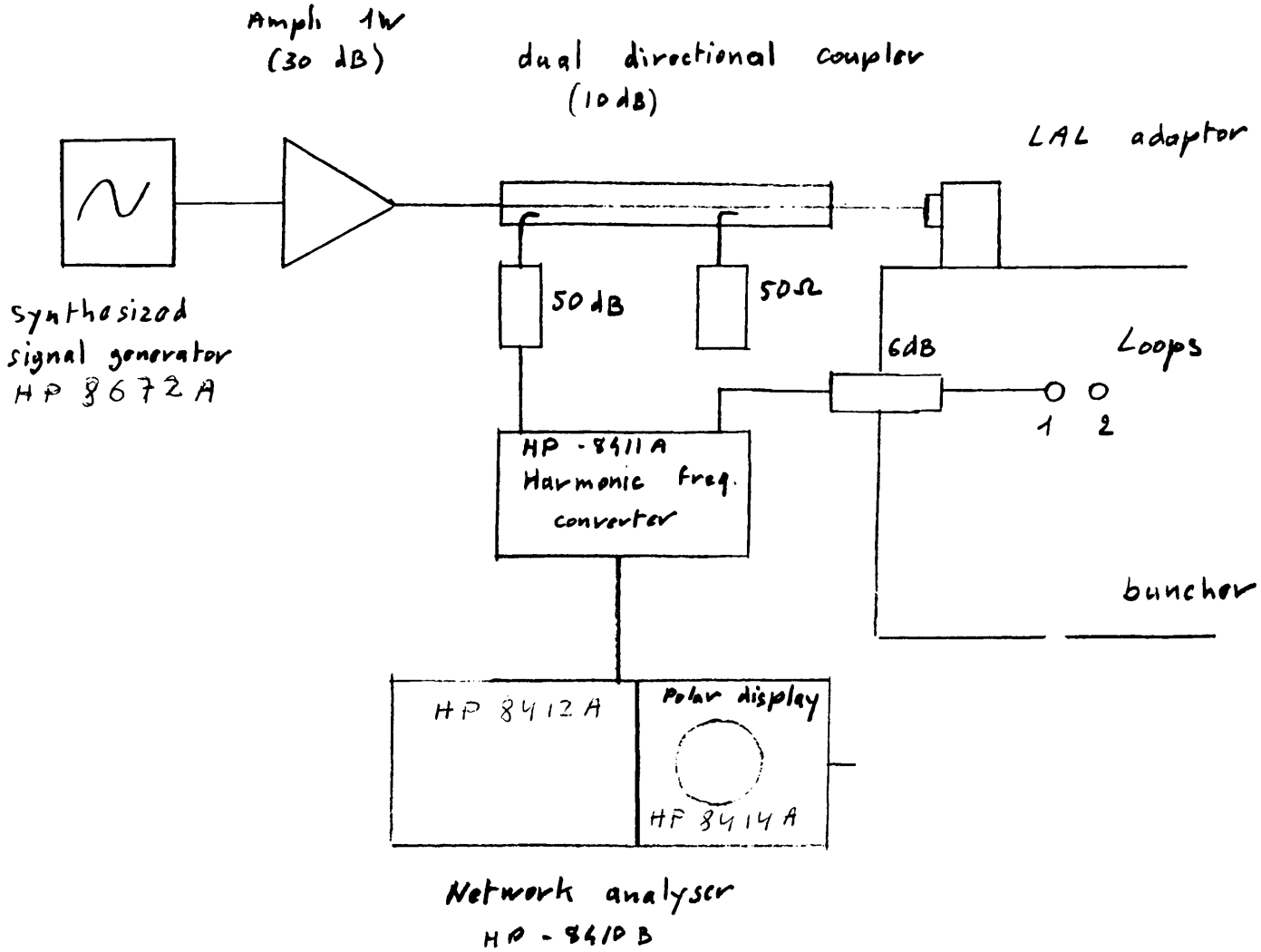


FIG.4. SCHEMATIC SET-UP FOR MODES MEASUREMENTS.

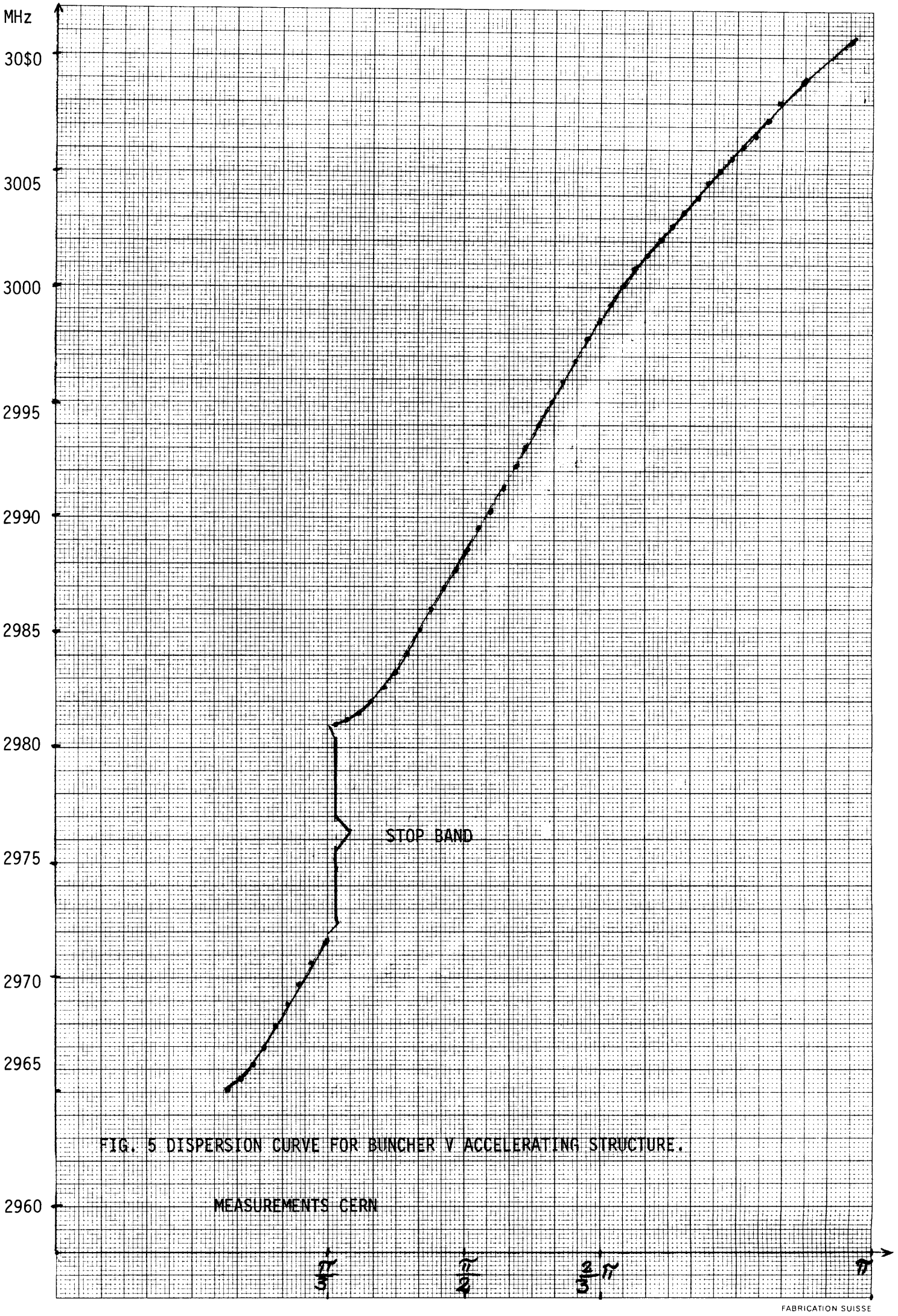


FIG. 5 DISPERSION CURVE FOR BUNCHER V ACCELERATING STRUCTURE.

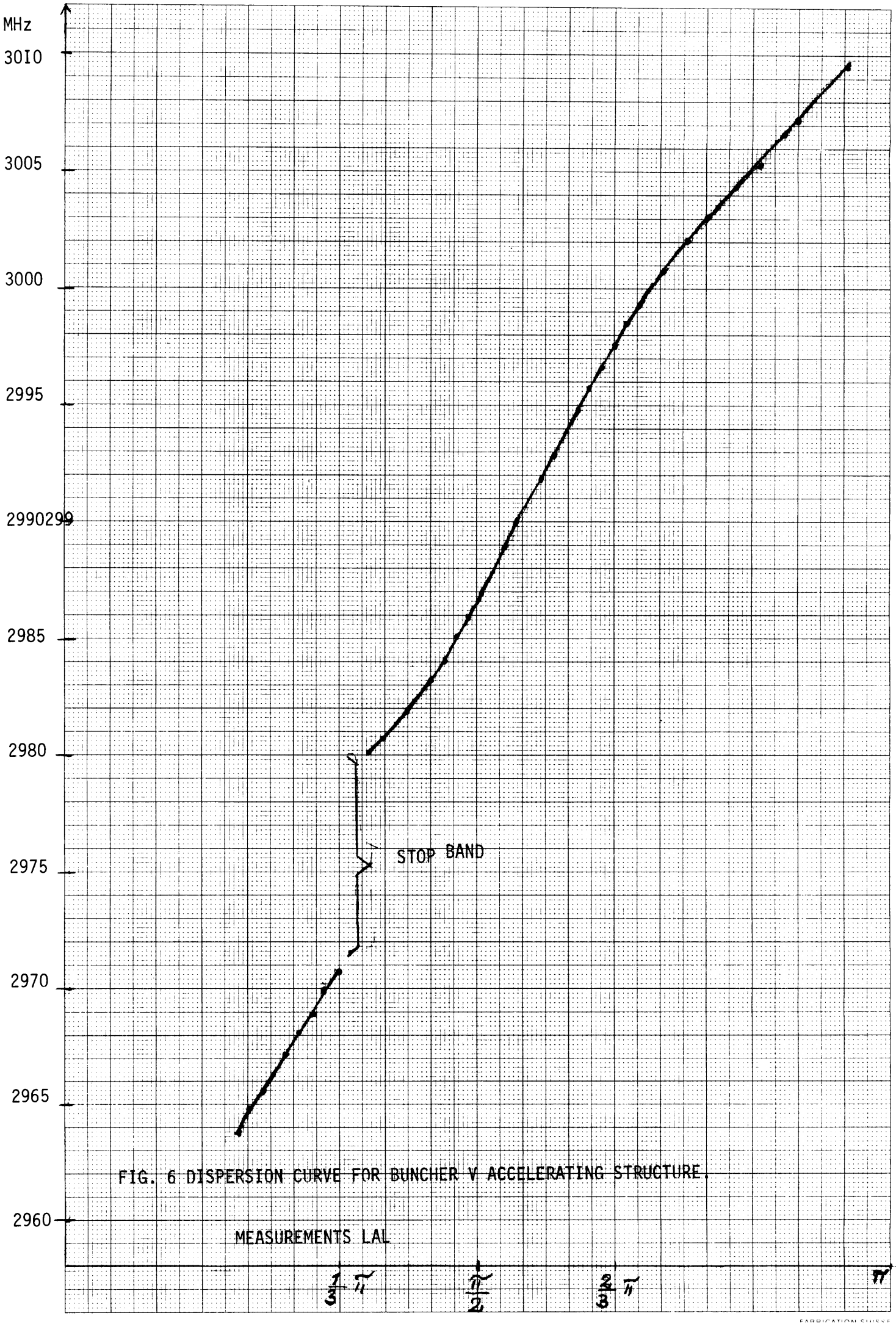


FIG. 6 DISPERSION CURVE FOR BUNCHER V ACCELERATING STRUCTURE.

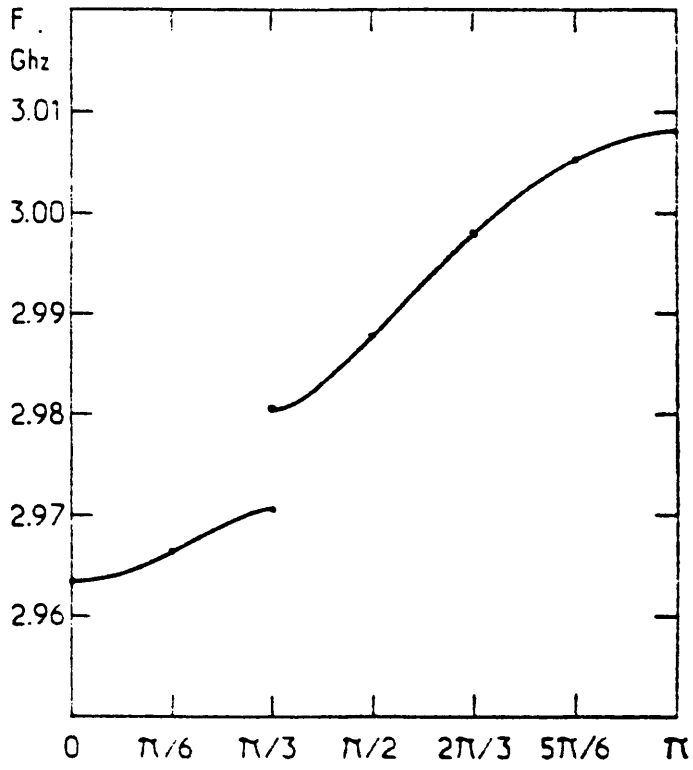


FIG. 7 DISPERSION CURVE FOR TRIPERIODIC ACCELERATING STRUCTURE OF CGR MEV MEASURED BY BENSUSSAN.

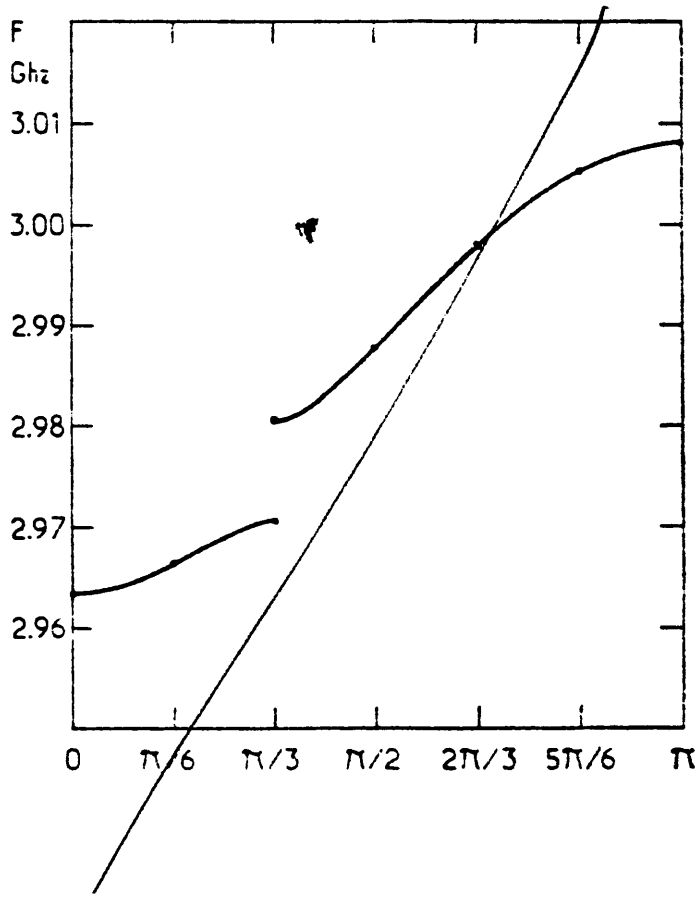
F
Ghz
3.01
3.00
2.99
2.98
2.97
2.96
0
π/6
π/3
π/2
2π/3
5π/6
π

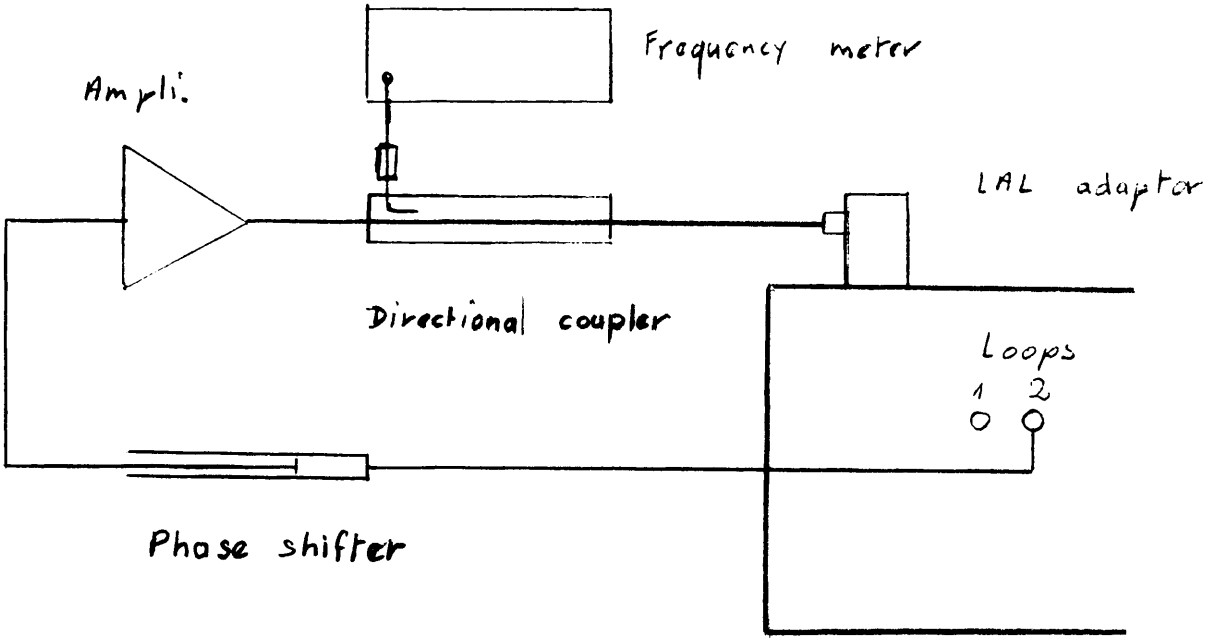


FIG. 8. MEASURING SET-UP FOR PERTURBATION MEASUREMENTS IN THE AUTOOSCILLATING MODE.

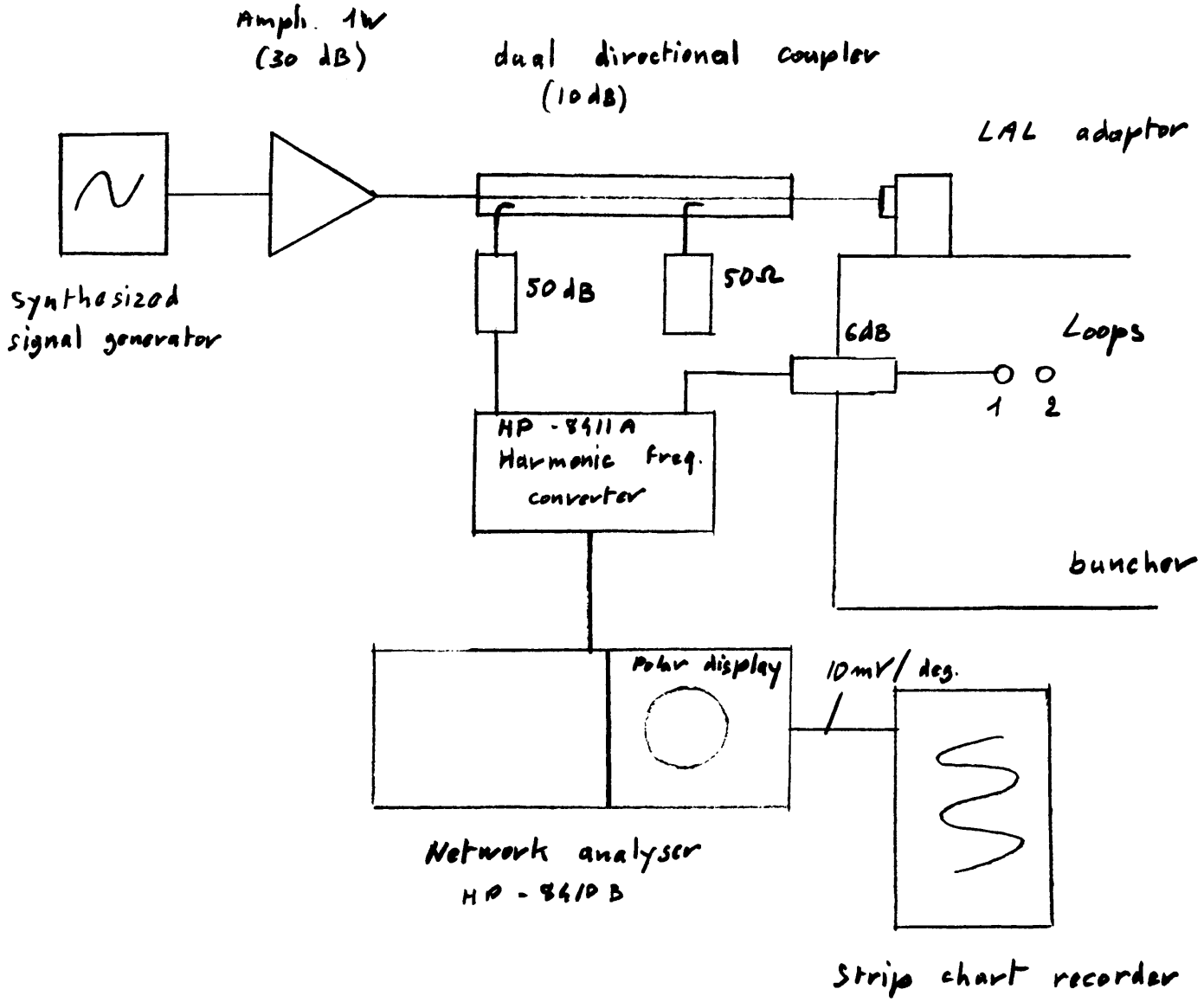


FIG. 9. SCHEMATIC DIAGRAM FOR PERTURBATION MEASUREMENTS VIA PHASE SHIFT.

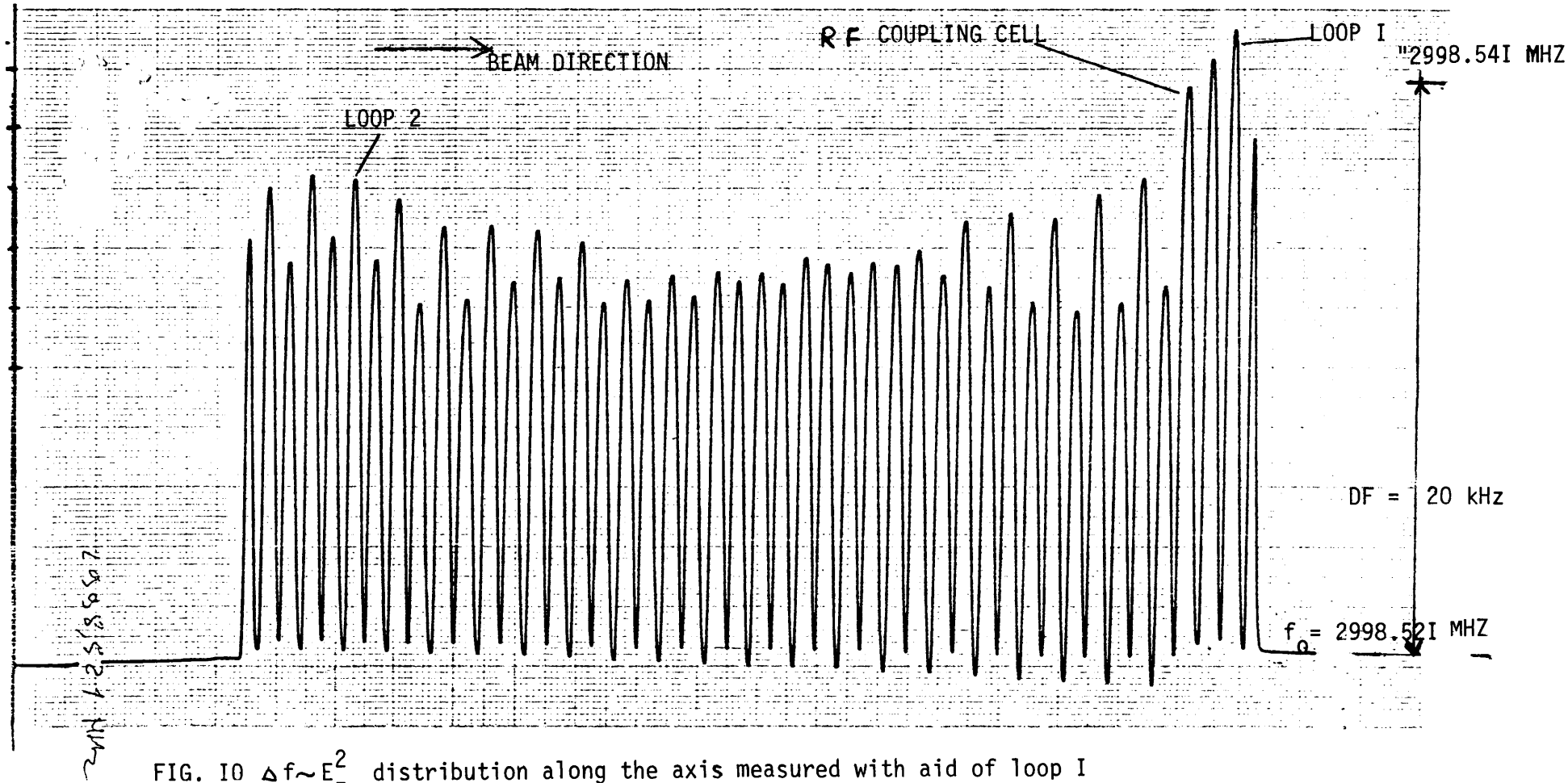


FIG. IO $\Delta f \sim E_z^2$ distribution along the axis measured with aid of loop I

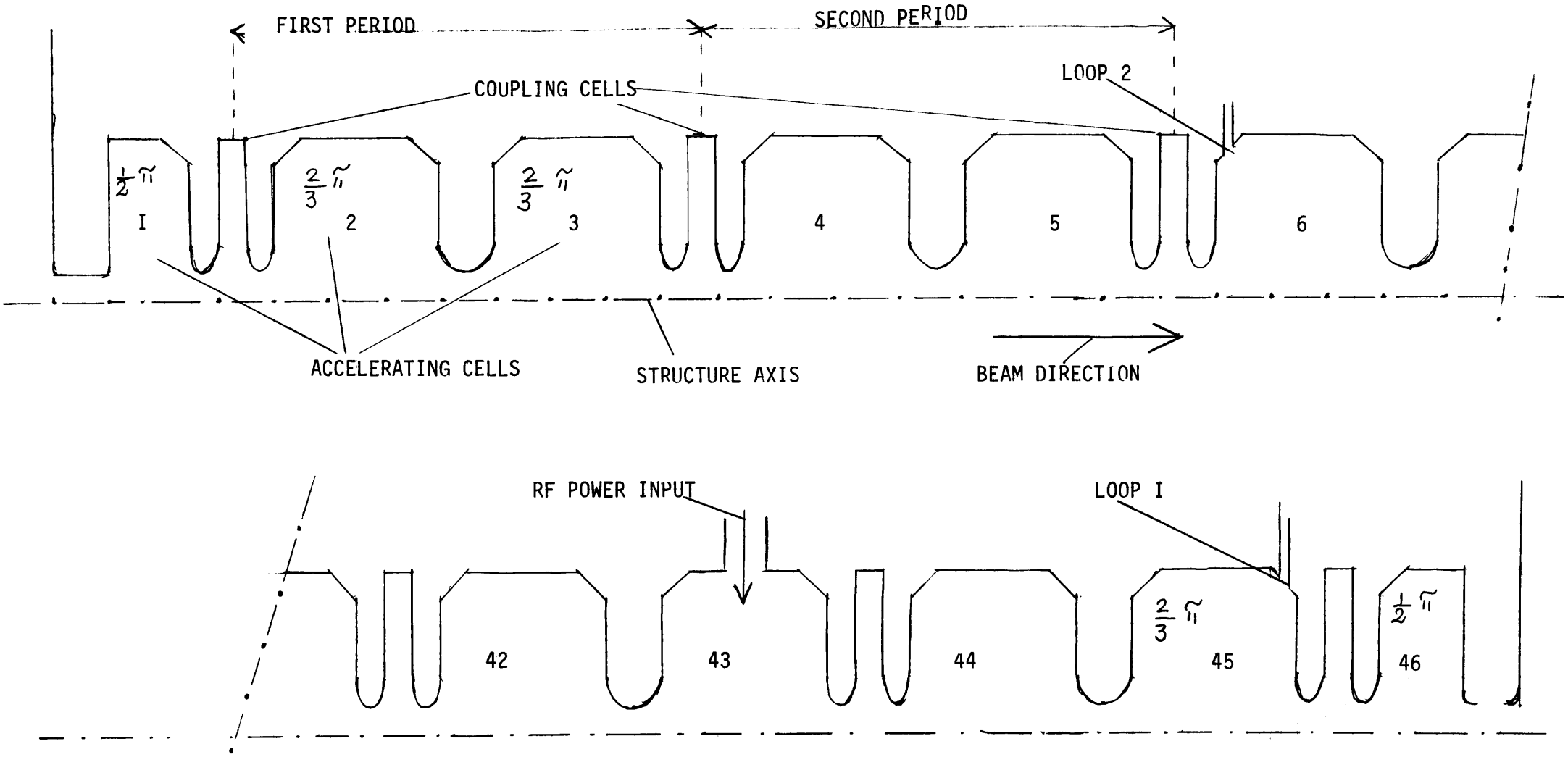


FIG. IOA. SCHEMATIC LAYOUT OF THE TRIPERIODIC STANDING WAVE BUNCHER V ACCELERATING STRUCTURE.

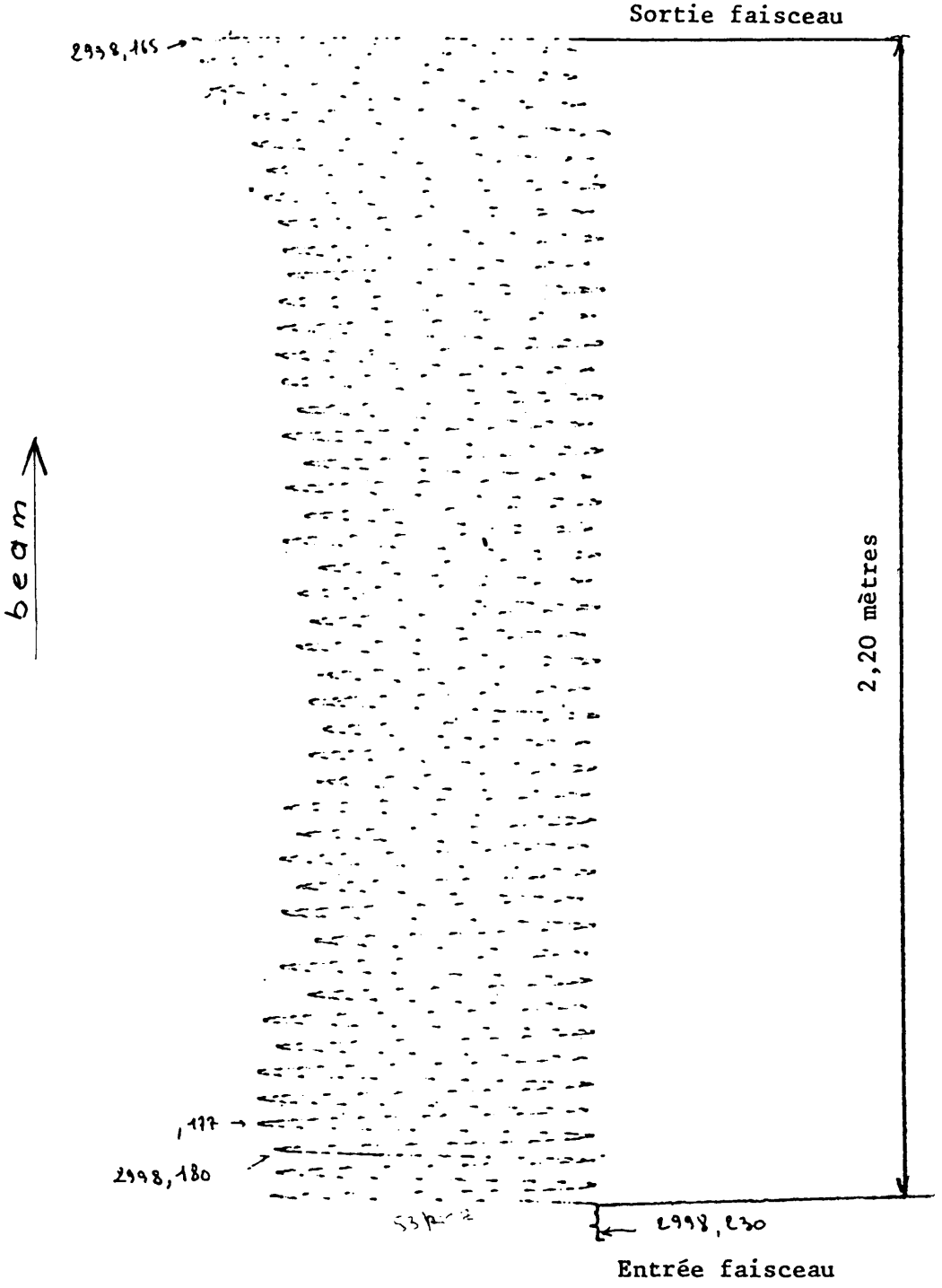


FIG. II $\Delta f \sim E_z^2$ DISTRIBUTION ALONG THE AXIS — MEASUREMENTS LAL.

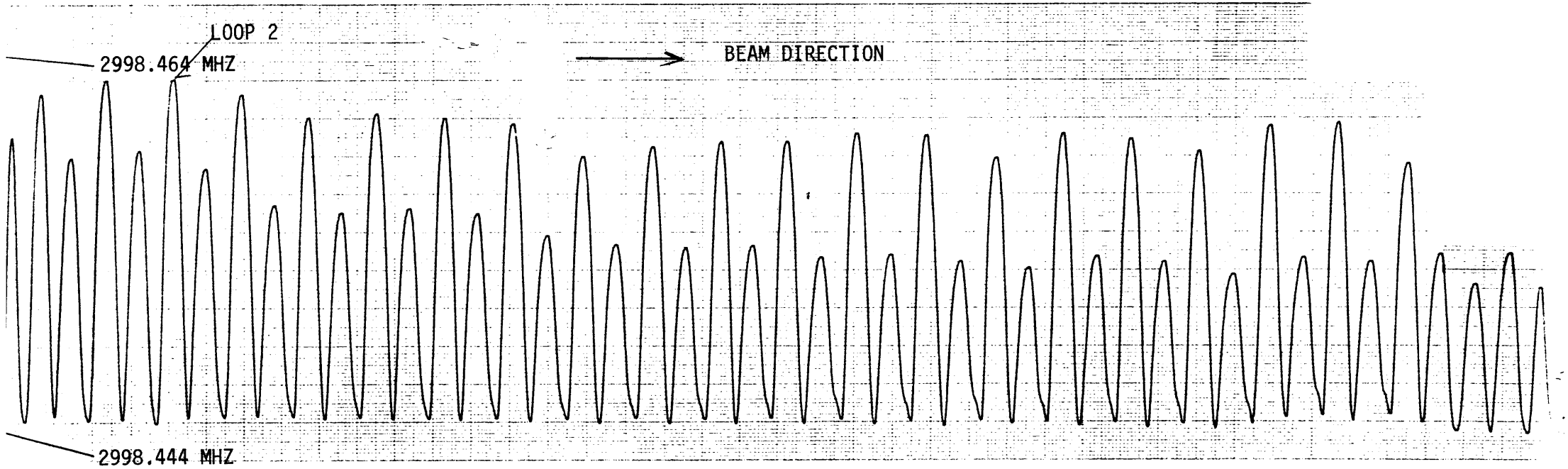


FIG .I2 $\Delta f \sim E_z^2$ DISTRIBUTION ALONG THE AXIS MEASURED WITH AID OF LOOP 2

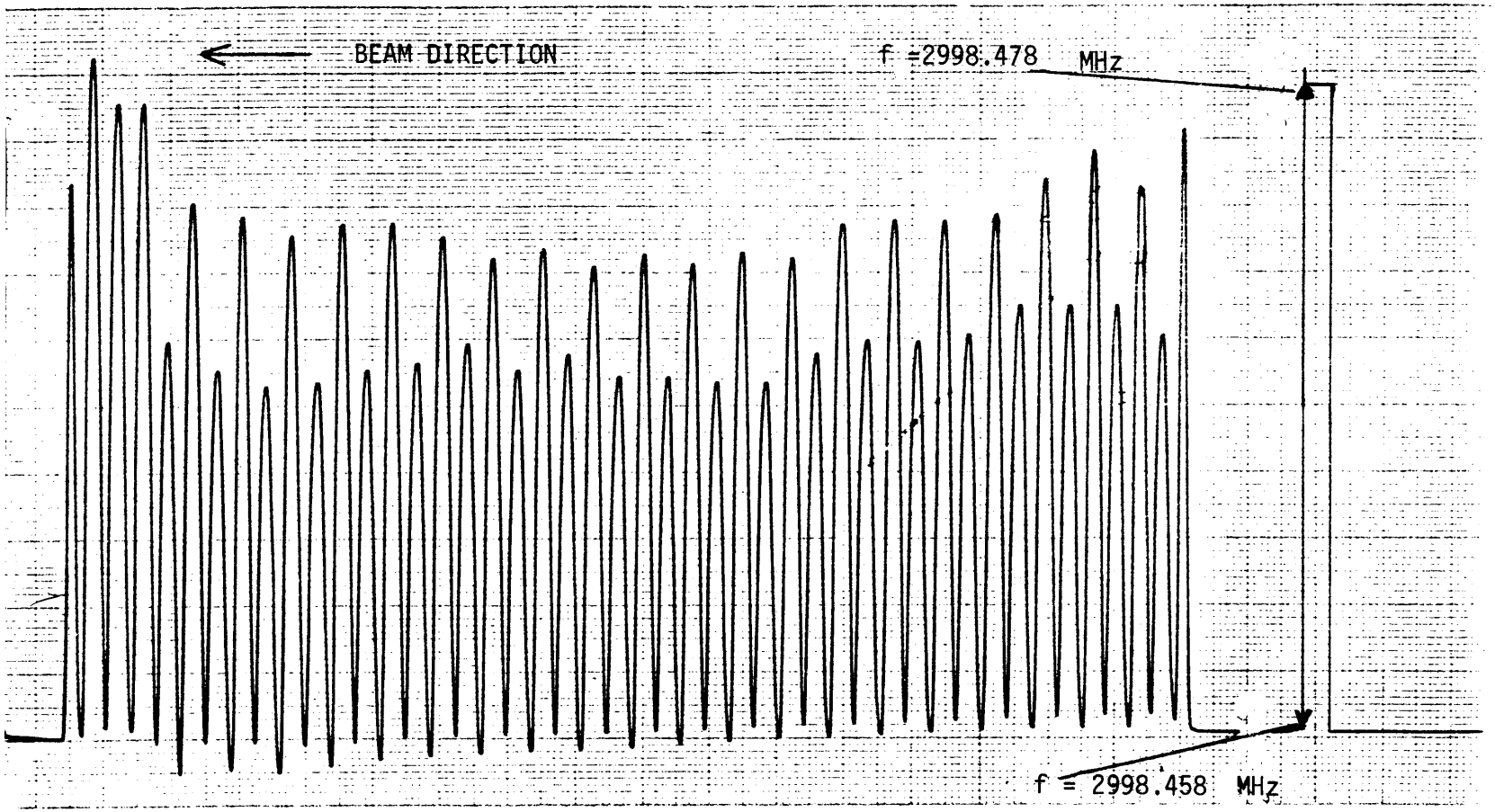


FIG. I3 $\Delta f \sim E_z^2$ DISTRIBUTION ALONG THE AXIS FOR $\Delta f$=-63 kHz FREQUENCY SHIFT.

PERTURBATION AT THE BEGINNING OF THE STRUCTURE

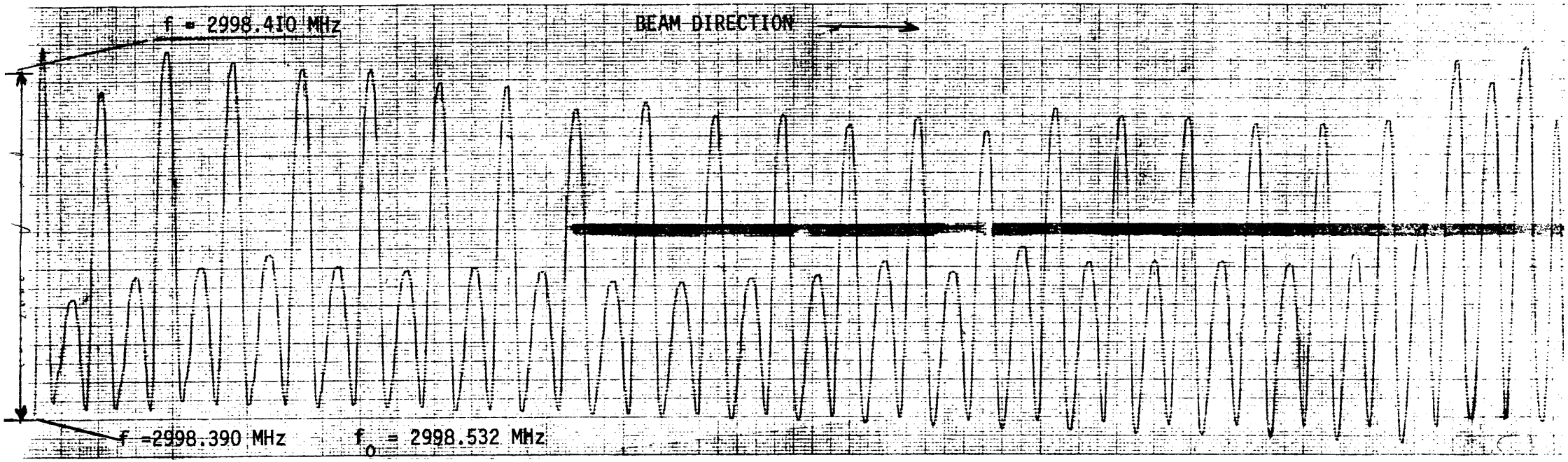


FIG. I4 $\Delta f \sim E_z^2$ DISTRIBUTION ALONG THE AXIS FOR $\Delta f$ = -I30 kHz FREQUENCY SHIFT PERTURBATION AT THE BEGINNING OF THE STRUCTURE.

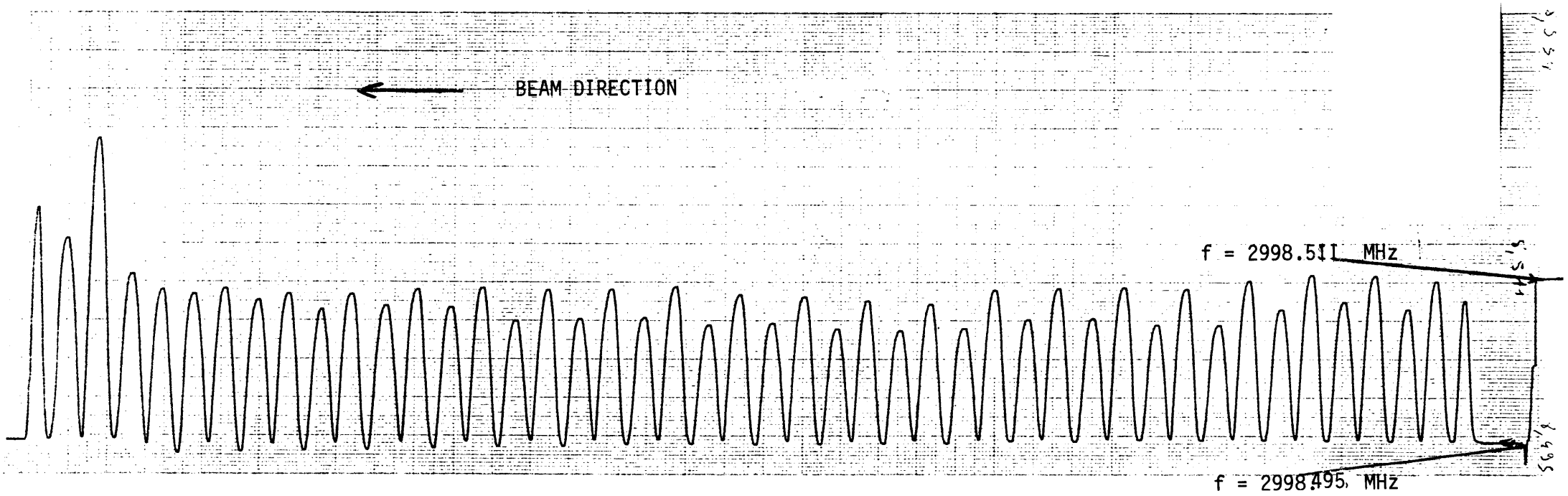


FIG. I5 $\Delta f \sim E_z^2$ DISTRIBUTION ALONG THE AXIS FOR $\Delta f$=-40 kHz FREQUENCY SHIFT.

PERTURBATION AT THE END OF THE STRUCTURE.

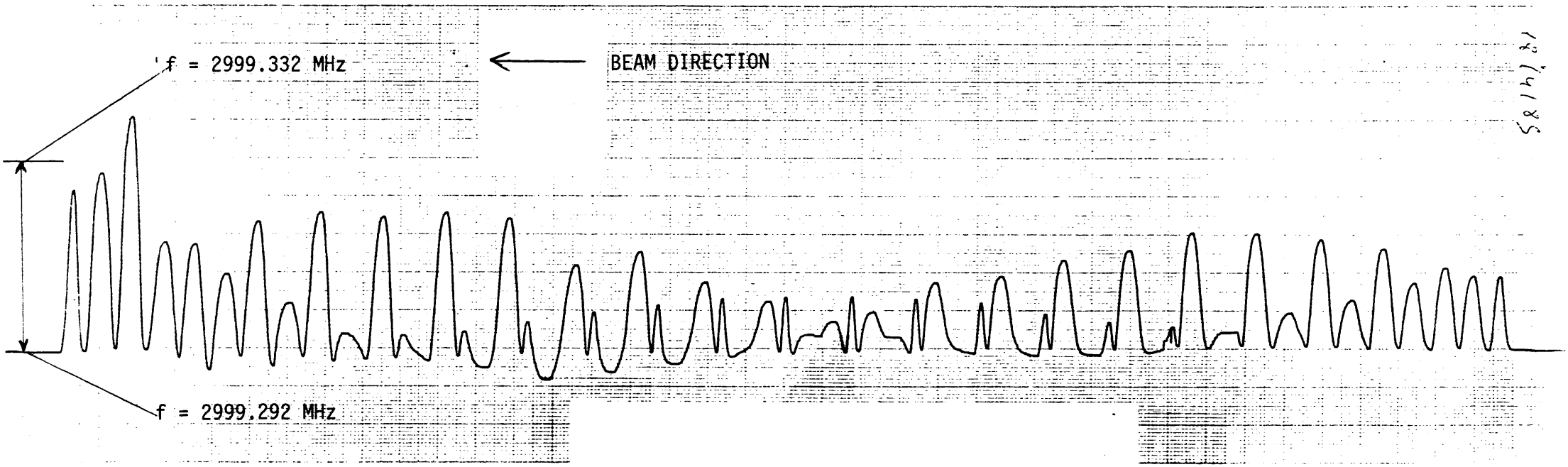


FIG. I6 $\Delta f \sim E_z^2$ distribution for the first higher adjacent mode.

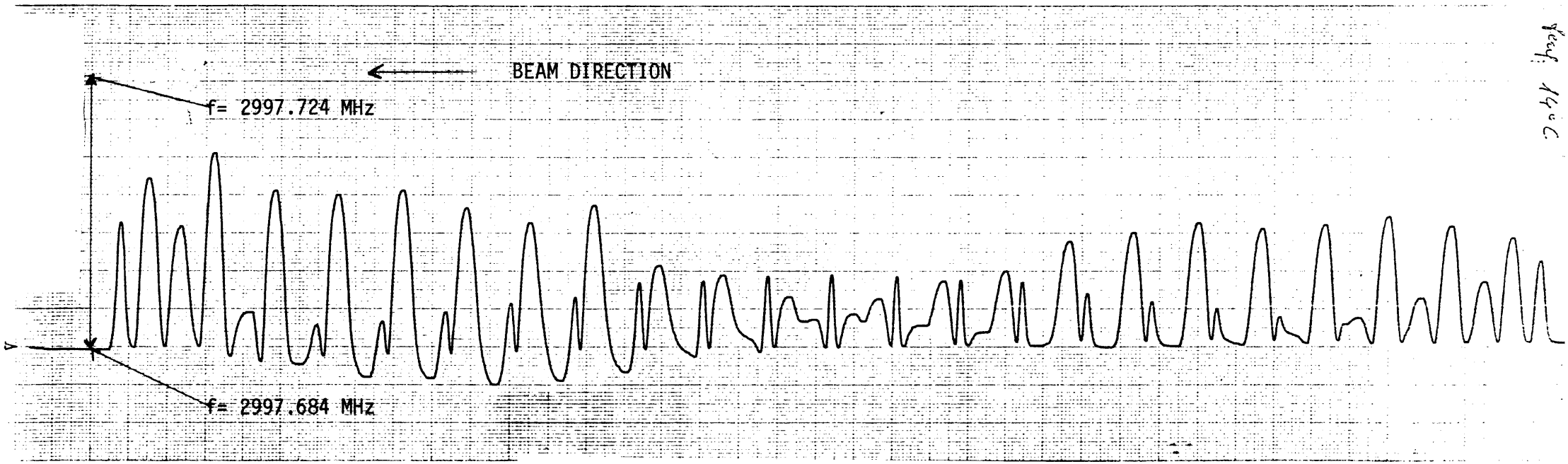


FIG. I7 $\Delta f \sim E_z^2$ DISTRIBUTION FOR THE FIRST LOWER ADJACENT MODE

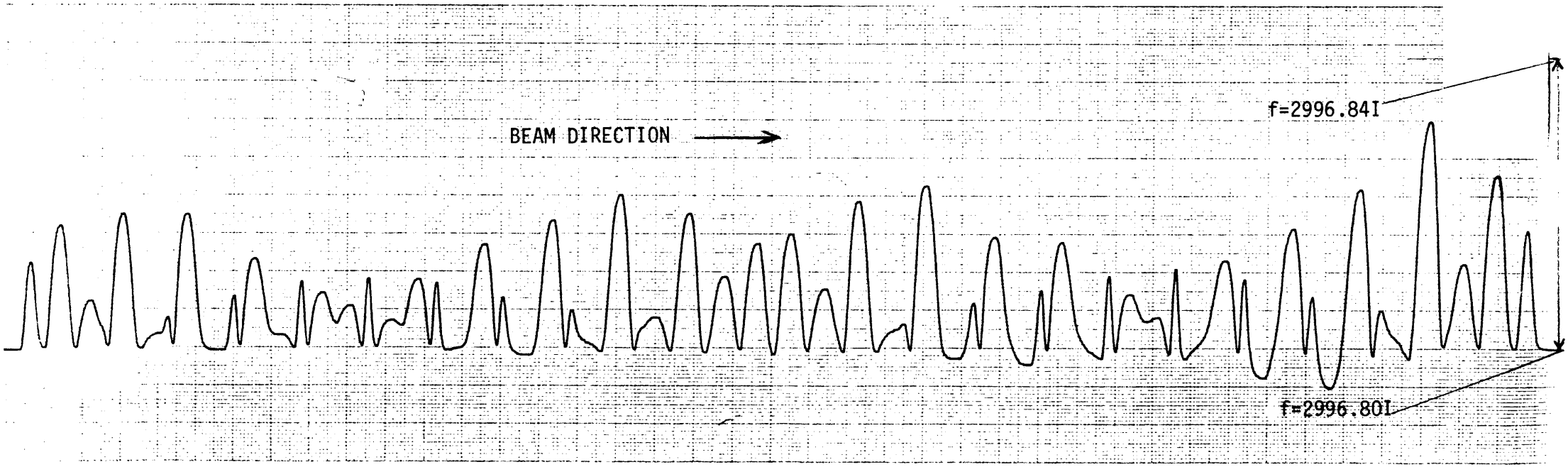


FIG. 18 $\Delta f \sim E_z^2$ DISTRIBUTION FOR THE SECOND LOWER ADJACENT MODE.